07

Effect of laser processing rate on silicon crystallization in a two-layer aluminum/silicon structure on a flexible polyimide substrate

© L.D. Volkovoynova, A.V. Kozlowski, V.V. Galushka, S.B. Venig, A.A. Serdobintsev

Saratov National Research State University, Saratov, Russia
E-mail: volkovoinovald@sgu.ru

Received September 5, 2024
Revised February 10, 2025
Accepted February 11, 2025

The effect of the processing rate of a two-layer thin-film aluminum/silicon structure on a flexible polyimide substrate by infrared pulsed laser radiation on its composition, crystal structure, and surface morphology has been studied. For this purpose, several lines with laser movement speeds of 100−300 mm/s were formed. The samples were studied by Raman scattering, energy-dispersive X-ray analysis, and atomic-force microscopy. A comprehensive study of the treated areas made it possible to identify up to seven regions differing in the structure of the silicon layer. During the study, it was found that some areas are completely crystallized or contain a mixture of crystalline and amorphous phases

Keywords: flexible electronics, silicon crystallization, metal-induced silicon crystallization, laser-induced silicon crystallization, infrared laser.

DOI: 10.61011/TPL.2025.05.61056.20106

Flexible electronics is one of the research fields that are developing rapidly at present. Such research covers the production of batteries, sensors, and electronic skin [1–4]. Amorphous silicon (*a*-Si) [5,6] is used to fabricate flexible electronic devices, since the production of polycrystalline silicon (*pc*-Si) is complicated by its high crystallization temperature, which exceeds the melting temperature of flexible polymer substrates. However, *pc*-Si has several advantages over *a*-Si. Specifically, the optical-electrical conversion efficiency for *a*-Si is as low as 14 %, while *pc*-Si has an efficiency of 22−26 % [7]. In order to mitigate the issue of destruction of flexible polymer substrates with *pc*-Si- coatings synthesized on them, we have developed the method of metal-induced laser-stimulated (MILS) crystallization of Si [8].

This technique allows one to produce *pc*-Si films with a reduced influence on the substrate, thereby preserving its integrity [8–10]. MILS crystallization involves the irradiation of a two-layer substrate/*a*-Si/metal structure with a pulsed infrared (IR) laser. The metal layer acts as an absorber, which then transfers energy to *a*-Si through heat transmission. Since *a*-Si and a polymer substrate are virtually transparent to IR radiation (the absorption coefficients of *a*-Si and polyimide (PI), which is used most often as a substrate material, at a wavelength of 1064 nm are 60.75 cm^{-1} [11] and 4.95 cm^{-1}, respectively [12]), IR radiation is absorbed by the metal layer only (for example, Al and Ni metals used in our studies [8–10] are characterized by absorption coefficients of $1.0927 \cdot 10^6$ [13] and $1.3854 \cdot 10^6$ cm^{-1} [14], respectively), which helps preserve the integrity of the flexible substrate. The aim of the present study is to examine in detail the influence of processing rate (laser beam scanning rate) on the process of MILS synthesis of *pc*-Si.

The studied samples were two-layer structures of *a*-Si (1 μm in thickness) and Al (100 nm in thickness) layers [7] deposited sequentially by magnetron sputtering onto a PI film with a thickness of 0.5 mm. These samples were fabricated using a Nexdep setup (Angstrom Engineering, Canada) fitted with two magnetron sources with disk targets 76 mm in diameter. The presence of two magnetron sources in the vacuum chamber provided an opportunity to deposit *a*-Si and Al layers without breaking the vacuum. The residual pressure in the chamber was no higher than $2 \cdot 10^{-5}$ Torr; prior to sputtering, argon with a purity of 99.999 % was fed into the chamber until a working pressure of $3.4 \cdot 10^{-3}$ Torr was reached.

Following sputtering, the samples were processed with pulsed laser radiation with a wavelength of 1064 nm and a spot diameter of 20 μm at a MiniMarker-2 setup (Laser Center, Russia). Five lines were formed on the sample by a single scan with the laser beam. Each line was formed at a certain scanning rate (100, 150, 200, 250, and 300 mm/s). The other radiation parameters were fixed: the pulse repetition rate was 99 kHz, the pulse duration was 100 ns, and the power was 0.2 W.

The structure of Si after laser processing was studied by the Raman scattering (RS) method using an InVia Raman microscope (Renishaw, UK). A laser with a wavelength of 532 nm was used. At a radiation power of 0.125 mW, the laser spot diameter was 1.3 μm. Raman spectra were recorded at 40 points across each line with a pitch of 1 μm.

The chemical composition of the samples after processing was examined with a Mira II LMU (Tescan, Czech Republic) scanning electron microscope (SEM) fitted with an energy dispersive analysis (EDX) attachment (Oxford Instruments, UK). The primary electron beam energy was 15 keV.

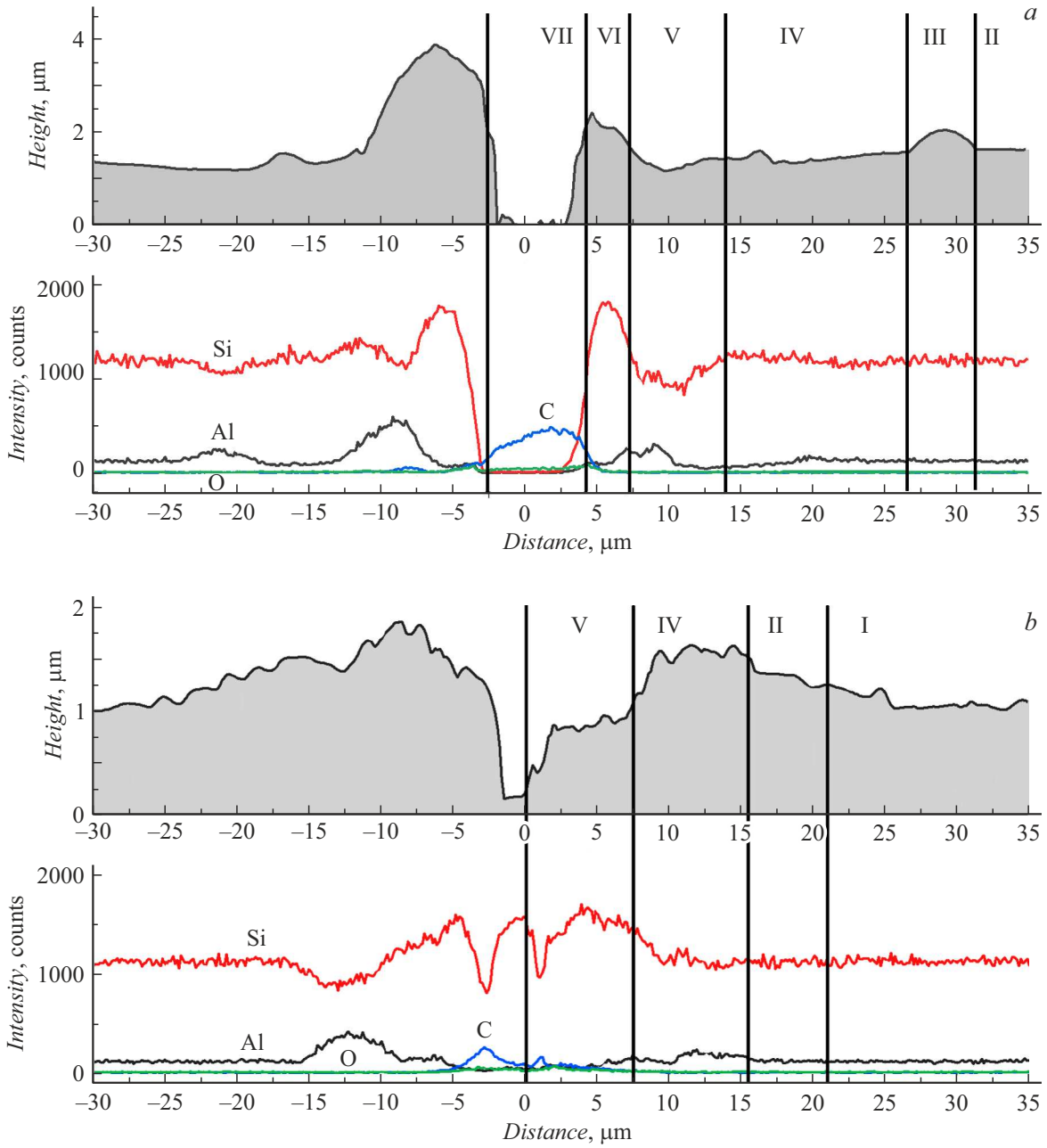


Figure 1. Comparison of surface (top) and composition (bottom) profiles for a line formed at a rate of 100 (*a*) and 300 mm/s (*b*).

The surface morphology was studied via atomic force microscopy (AFM) using an NTEGRA-Spectra (NT-MDT, Russia) probe station. A semi-contact scanning mode was set, and the resolution was 512 × 512 points. The scanning rate varied from 0.2 to 0.5 Hz. The obtained data were processed in Gwyddion 2.66.

The above research methods allowed us to perform a comprehensive analysis of the processed two-layer structures on a flexible PI substrate. Figure 1 presents a comparison of typical experimental AFM and EDX data obtained in transverse profiling of lines formed at the rates of 100 and 300 mm/s. The profiles are slightly asymmetric. This is likely attributable to the PI substrate flexibility, which leads to slight distortions of laser beam focusing during processing. It should be noted that the AFM and EDX profiles are combined in a somewhat arbitrary manner, since accurate positioning at the same sample site at two different setups is impossible. Therefore, Fig. 1 shows the most typical profiles for the studied samples.

Figure 2 shows SEM images of sections of lines obtained at the rates of 100 and 300 mm/s. A region of exposed polyimide at the center of the line obtained at a laser scanning rate of 100 mm/s is visible in Fig. 2, *a*. Similar small regions are also present at the center of the line formed

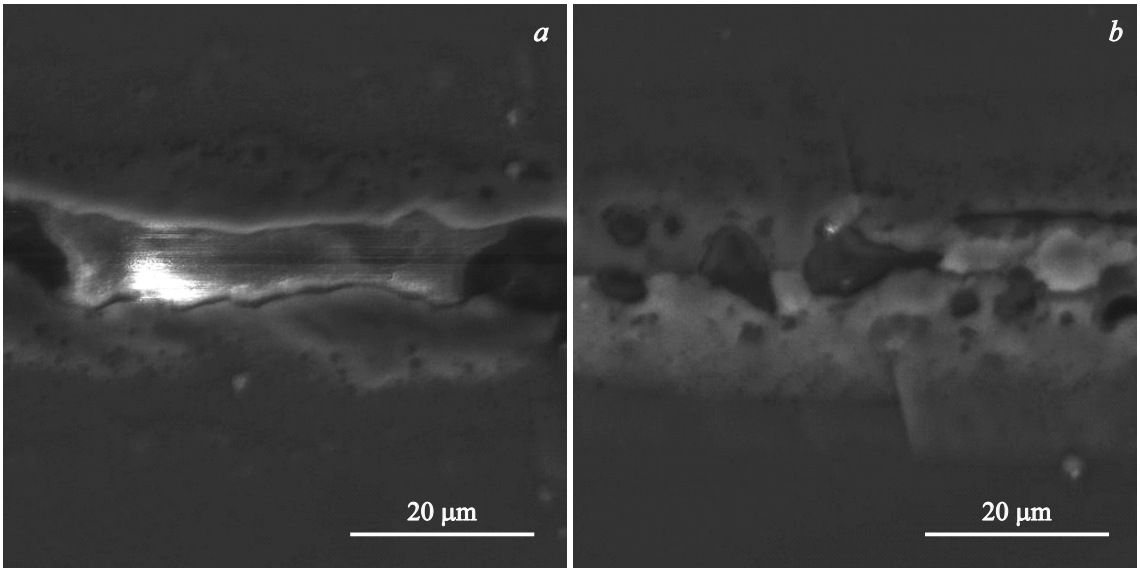


Figure 2. SEM images of lines formed at a rate of 100 (a) and 300 mm/s (b).

at a rate of 300 mm/s (Fig. 2, b). Beads of solidified material are seen around the lines, which is consistent with the AFM profiles (Fig. 1).

Up to seven regions in the vicinity of the formed lines differing in structure and composition could be identified based on the results of Raman, AFM, and EDX measurements. Note that a visual inspection of the SEM images of lines (Fig. 2) reveals a much smaller number of regions; therefore, the results of Raman, AFM, and EDX experiments formed the basis of data for analysis. The regions are designated by Roman numerals in Fig. 1: region I corresponds to the sample surface area that is not affected by laser irradiation, while region VII is located directly at the center of the line. The lowest laser scanning rate (100 mm/s) corresponds to the highest energy of laser radiation absorbed by the sample, since the distance between adjacent pulses is minimal. Therefore, the laser-modified region was so large at this scanning rate that region I ended up outside the scan boundaries (Fig. 1, a). As the rate increases (and, consequently, the absorbed energy of laser radiation decreases), some of the regions disappear and the modified region becomes narrower. Specifically, only four regions remain identifiable for the 300 mm/s line (maximum laser scanning rate, minimum absorbed energy; see Fig. 1, b).

Figure 3 illustrates the variation of boundaries of the regions with an increase in laser scanning rate. The $1/e^2$ laser spot radius is also indicated.

Since the laser beam has a Gaussian distribution, the absorbed energy maximum is at the center of the processed line, where Al and Si are removed completely and the PI substrate is exposed (Fig. 3, a). Region VII is formed this way. Region VI is detected only at the minimum laser scanning rate and is characterized by the presence of both PI peaks and the TO mode peak of *pc*-Si. This region forms due to the fact that the *pc*-Si layer is damaged at high absorbed energy levels. With a pulse duration of 100 ns, a bead of *pc*-Si ejected to the periphery by steam pressure forms along the edges of the regions exposed to laser radiation [15]. This is how region V, which features an intense signal of the TO mode of *pc*-Si and no signals from *a*-Si, is detected. The concentration of Al in region V of the sample formed at a laser scanning rate of 100 mm/s and in region IV of the 300 mm/s sample exceeds slightly the concentration of Al in the original sample (Fig. 1). This is attributable to the transfer of ablated Al from region VII, which contributes to the formation of beads at the line edges, and is seen in the AFM profiles in Fig. 1.

The Raman signal from the TO mode of *pc*-Si in region IV is less intense than in region V; decomposition of the peak reveals a component that may probably be attributed to nanocrystalline silicon (*nc*-Si) with a crystallite size of 1–2 nm [16]. Region IV lies almost entirely outside the laser spot and, consequently, receives energy only through heat transfer across the Si layer. However, this energy was sufficient for partial crystallization of the Si- layer.

Region III is characterized by the Raman spectrum of *a*-Si with added *nc*-Si and *pc*-Si, while only *a*-Si and *nc*-Si are found in region II. In these two regions, the following known FWHM parameters (mode half-width) were used to isolate the peaks: 63 cm^{-1} for *a*-Si [17] and 30 cm^{-1} for the TO mode of the *nc*-Si peak. Region III is transitional and is detected only at low laser scanning rates (100–200 mm/s). Regions II and III are characterized by the same Al and Si content as untreated region I. Thus, it may be concluded that the Al layer in these regions is not ablated, but is damaged due to thermal exposure. This allows one to record the Raman signal from Si through gaps in the damaged Al layer.

It can be seen from Fig. 3 that region VII may be minimized by increasing the processing rate. This suggests

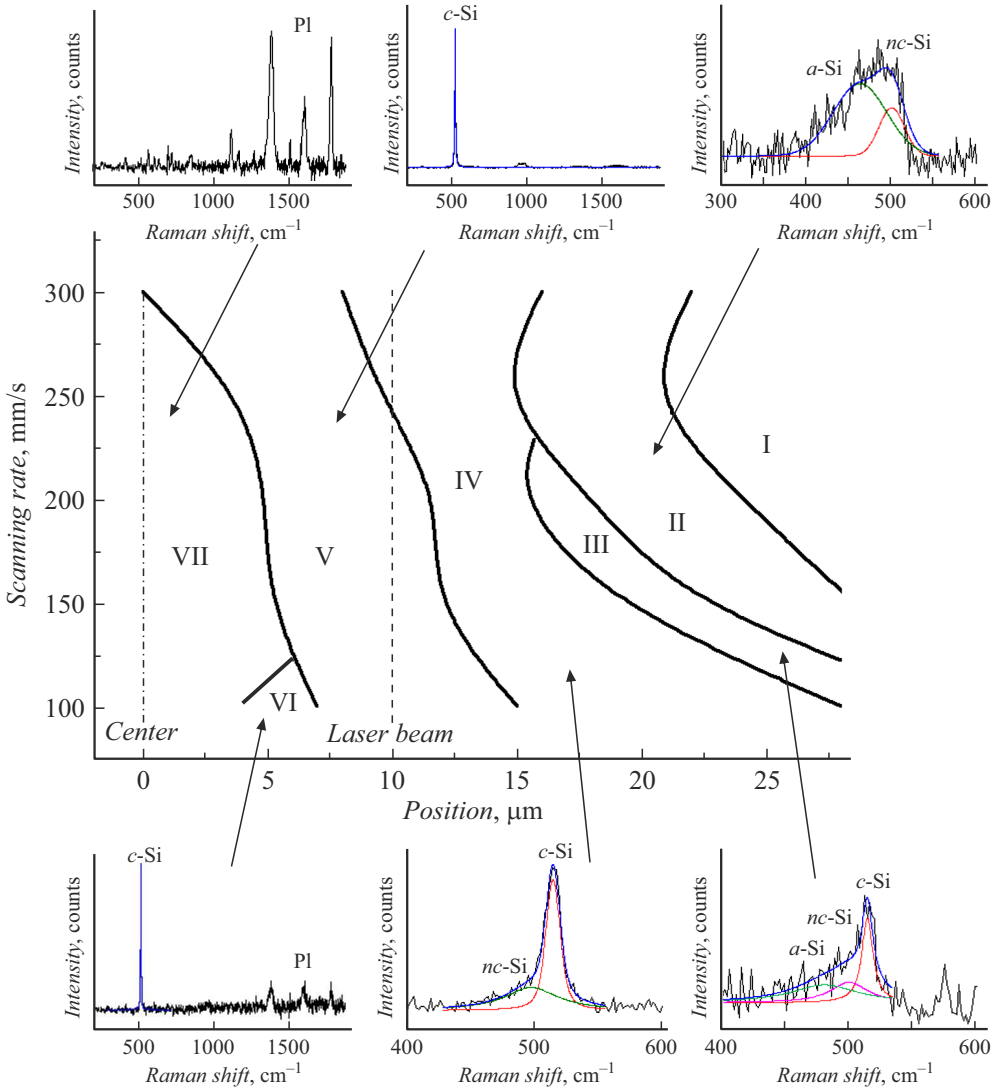


Figure 3. Changes in the boundaries of regions induced by laser processing rate variations. The insets show typical Raman spectra for certain regions. The dashed line indicates the laser spot radius.

that large-area continuous *pc*-Si- coatings may be obtained by MILS synthesis on flexible substrates.

Seven regions differing in their structure and composition were identified as a result of a comprehensive study of two-layer Al/Si samples on a flexible PI substrate processed with an IR laser. An explanation was proposed for the processes accompanying the irradiation of this structure. The validity of this explanation was verified by experimental data. The essence of the proposed mechanism is as follows. Both Al and Si are ablated in the region receiving the maximum irradiating laser beam energy, and PI is exposed there. A completely crystallized bead forms in this case. A fraction of evaporated Al is deposited back onto the sample surface at the boundary of the laser spot. Si crystallization was also observed outside the laser spot, which is attributable to heat transfer processes. It was demonstrated that pulsed IR laser irradiation of a two-layer Al/Si structure provides an opportunity to form extended *pc*-Si regions and preserve the integrity of a PI substrate.

Funding

This study was supported financially by the Russian Science Foundation, project No. 23-22-00047 (https://rscf.ru/project/23-22-00047/).

Conflict of interest

The authors declare that they have no conflict of interest.

References

[1] S.A. Hashemi, S. Ramakrishna, A.G. Aberle, Energy Environ. Sci., **13**, 685 (2020). DOI: 10.1039/c9ee03046h

[2] W. Liu, Y. Liu, Z. Yang, C. Xu, X. Li, Nature, **617**, 717 (2023). DOI: 10.1038/s41586-023-05921-z
[3] J.H. Jang, S. Li, D.-H. Kim, J. Yang, M.K. Choi, Adv. Electron. Mater., **9** (9), 2201271 (2023). DOI: 10.1002/aelm.202201271
[4] K.-N. Wang, Z.-Z. Li, Z.-M. Cai, L.-M. Cao, npj Flex. Electron., **8**, 33 (2024). DOI 10.1038/s41528-024-00318-y
[5] J.Y. Lee, J.E. Ju, C. Lee, S.M. Won, K.J. Yu, Int. J. Extr. Manuf., **6** (4), 042005 (2024). DOI: 10.1088/2631-7990/ad492e
[6] S. Kim, V.Q. Hoang, C.W. Bark, Nanomaterials, **11** (11), 2944 (2021). DOI: 10.3390/nano11112944
[7] H. Kang, IOP Conf. Ser.: Earth Environ. Sci., **726**, 012001 (2021). DOI: 10.1088/1755-1315/726/1/012001
[8] A.A. Serdobintsev, I.O. Kozhevnikov, A.V. Starodubov, P.V. Ryabukho, V.V. Galushka, A.M. Pavlov, Phys. Status Solidi A, **216**, 1800964 (2019). DOI: 10.1002/pssa.201800964
[9] A.A. Serdobintsev, A.M. Kartashova, P.A. Demina, L.D. Volkovoynova, I.O. Kozhevnikov, V.V. Galushka, Tech. Phys., **69** (3), 469 (2024).
[10] A.A. Serdobintsev, A.M. Kartashova, P.A. Demina, L.D. Volkovoynova, I.O. Kozhevnikov, Phys. Solid State, **65** (12), 2046 (2023). DOI: 10.61011/PSS.2023.12.57660.5111k.
[11] D. Franta, D. Nečas, L. Zajíčková, I. Ohlídal, J, Stuchlík, Thin Solid Films, **541**, 12 (2013). DOI: 10.1016/j.tsf.2013.04.129
[12] R.H. French, J.M. Rodríguez-Parada, M.K. Yang, R.A. Derryberry, M.F. Lemon, M.J. Brown, C.R. Haeger, S.L. Samuels, E.C. Romano, R.E. Richardson, in *2009 34th IEEE Photovoltaic Specialists Conf. (PVSC)* (IEEE, 2009), p. 000394. DOI: 10.1109/PVSC.2009.5411657
[13] K.M. McPeak, S.V. Jayanti, S.J.P. Kress, S. Meyer, S. Iotti, A. Rossinelli, D.J. Norris, ACS Photon., **2**, 326 (2015). DOI: 10.1021/ph5004237
[14] W.S.M. Werner, K. Glantschnig, C. Ambrosch-Draxl, J. Phys. Chem. Ref. Data, **38**, 1013 (2009). DOI: 10.1063/1.3243762
[15] D.S. Polyakov, A.A. Shamova, G.D. Shandybina, *Vzaimodeistvie lazernogo izlucheniya s veshchestvom. Fiziko-khimicheskie protsessy v kondensirovannykh sredakh, initsiirovannye lazernym nagrevom* (ITMO, SPb., 2023) (in Russian).
[16] S.V. Gaisler, O.I. Semenova, R.G. Sharafutdinov, B.A. Kolesov, Phys. Solid State, **46** (8), 1528 (2004). DOI: 10.1134/1.1788789.
[17] I.E. Tyschenko, V.A. Volodin, Semiconductors, **46** (10), 1286 (2012). DOI: 10.1134/S106378261210018.

Translated by D.Safin